metals

MDPI

Article

Optimisation of Heat Treatment Process for Damping Properties of Mg-13Gd-4Y-2Zn-0.5Zr Magnesium Alloy Using Box–Behnken Design Method

Jun Zhang [1,2,*], Ziming Kou [1], Yaqin Yang [3], Baocheng Li [3], Xiaowen Li [3], Ming Yi [3] and Zhongjian Han [3]

1 College of Mechanical Engineering, Taiyuan University of Technology, Taiyuan 030024, China; xiangyangzitian@163.com
2 Beijing Research Institute of Precise Mechatronic Controls, Beijing 100076, China
3 College of Materials Science and Engineering, North University of China, Taiyuan 030051, China; yangyaqin@nuc.edu.cn (Y.Y.); libaocheng@nuc.edu.cn (B.L.); nuc_lixiaowen@126.com (X.L.); schoolofblueshit@163.com (M.Y.); hzj4965@163.com (Z.H.)
* Correspondence: zhangjun0421@163.com; Tel.: +86-351-3921778

Received: 10 December 2018; Accepted: 27 January 2019; Published: 1 February 2019

Abstract: High damping magnesium alloys have poor mechanical properties, so it is necessary to investigate the damping properties of high-strength wrought magnesium alloys to effectively reduce vibration and noise in mechanical engineering. The aim of this work is to improve the mechanical damping performance of a novel high-strength Mg-13Gd-4Y-2Zn-0.5Zr magnesium alloy by optimising the heat treatment process. The mechanical damping coefficient, considering not only damping capacity but also the yield strength, is selected as one of the evaluation indexes. The other evaluation index is the tensile strength. The solid solution and ageing treatment were optimised by Box-Behnken method, an efficient experimental design technique. Heat treatment experiments based on the optimal parameters verified that the best process is a solution at 520 °C for 10 h followed by ageing at 239 °C for 22 h. The damping coefficient reaches 0.296, which is 73.1% higher than that before heat treatment. There was a good agreement between the experimental and Box-Behnken predicted results. The microstructure, morphology and composition of the second phases after heat treatment were analysed by SEM, XRD and EDS. Due to the high content of alloying elements in Mg-13Gd-4Y-2Zn-0.5Zr alloy, there are a large number of second phases after heat treated. They mainly include layer, short rod-shaped, bulk long period stacking order (LPSO) $Mg_{12}YZn$ and granular Mg_5Gd phases. It was found that the area fraction of the second phases has an extreme effect on the damping capacity and short rod-shaped LPSO can effectively improve the damping capacity of heat-treated Mg-13Gd-4Y-2Zn-0.5Zr alloy. The volume fraction of the second phases was analysed by ImageJ software. It was concluded that the smaller the area occupied by the second phases, the better the mobility of the dislocation, and the better the damping performance of the alloy. The statistical analysis results obtained using ImageJ software are consistent with the experimental results damping capacity.

Keywords: Mg-13Gd-4Y-2Zn-0.5Zr magnesium alloy; Box-Behnken design method; damping capacity; mechanical damping coefficient; solid solution and ageing treatment; LPSO phase; volume fraction of the second phases

1. Introduction

With the development of mechanical engineering, mechanical equipment now tends to be efficient and automated. However, problems caused by vibration, noise and fatigue fracture are becoming

increasingly prominent. Vibration and noise seriously hamper the stability and reliability of mechanical equipment operation. The development and application of damping materials with high damping capacity is an effective way to reduce vibration and noise in engineering. In theory, the performance of vibration and noise reduction is determined by the internal friction of metal, and the value of damping capacity is always being used to evaluate it. The damping capacity of a material refers to its ability to convert mechanical vibration energy into thermal energy. High damping capacity has been one of the most important properties of materials used in engineering structures [1].

Magnesium alloys not only have excellent high specific strength and high specific stiffness, but they also have a higher damping capacity than aluminium alloys, titanium alloys and steels. The damping coefficient of magnesium alloys is 15 times that of aluminium alloys and 60 times that of steels. The traditional view about damping capacity of Mg alloys conforms to Granato-Lücke (G-L) dislocation damping theory. According to G-L theory, the damping capacity of Mg is only related to the movement of basal dislocation, which relies on internal friction caused by vibration stress. Generally, in high damping alloys, dislocations are relatively free to vibrate [2]. However, high damping magnesium alloys always have poor mechanical properties; for example, the yield strength of high damping as-cast Mg-0.4Zn-0.6Zr alloy is only 50–60 MPa, which has greatly limited their application [3,4]. So it is much more important to comprehensively analyse the damping capacity and the strength of the commonly used high-strength magnesium alloys at the same time, rather than just considering high damping capacity. Research shows that Mg-RE alloys generally have good comprehensive mechanical properties. High-strength Mg-RE alloys generally contain Gd and Y as alloying elements. Mg-Gd-Y alloys not only have high strength and toughness, but they also have high corrosion resistance and good mechanical properties at high temperature. For example, the yield strength of as-cast novel Mg-13Gd-4Y-2Zn-0.5Zr alloy is up to 200 MPa [5–7], which can be widely used in instruments, meters, and the automotive industry. Therefore, it is necessary to study the damping properties of this alloy to improve its vibration and noise reduction.

Heat treatment can improve the mechanical properties of alloys by controlling the material's microstructure. Damping properties can also be improved because heat treatment can affect the solid solution atom, grain size, point defect, dislocation entanglement, morphology, size, the quantity of the precipitate phase, which can affect movements of dislocation in the alloy. After solution treatment, the strengthening element is present in the magnesium matrix in the form of solute atoms. Dislocations can be relatively easy to get rid of the pinning of solute atoms, which are usually considered to be weak pinning points. After ageing treatment, the strengthening element is present in the magnesium matrix in the form of precipitated phases, such as $Mg_{17}Al_{12}$ phases in the AZ91D alloy. Dislocation is difficult to get rid of the strong pinning effect of the precipitation phase and the damping capacity of magnesium alloys decreases. Zhang et al. [8] found that after annealing, the hot rolled Mg-0.6Zr alloy exhibited good damping properties, and it increased with the annealing time. Annealing causes the dislocation entanglement which is formed in the hot-rolling process of the alloy to disappear, and the density of the movable dislocations is increased. In addition, as the annealing time increases, the crystal grains will grow to a certain extent, which will reduce the number of grain boundaries and make the dislocation movement easier. Liu et al. [9] found that after solution treatment, the damping of ZK40-2.5NdCd was greater than that of cast alloy, mainly because MgZn compounds precipitated during the cooling process, and the content of Zn in the matrix decreased. Thus, a reasonable heat treatment process can effectively improve the contradiction between the mechanical and damping properties of the alloy. Research into the heat treatment process is of great significance for the development of high-strength vibration-damping metal materials.

Heat treatment is related to factors such as solution temperature, solution time, ageing temperature and ageing time. During the heat treatment process, different combinations of temperature and time will cause different microstructures and mechanical properties. The more factors that affect an experiment, the more cumbersome the combinations and the bigger the workload, which lead to

low efficiency and a waste of resources. Therefore, it is especially important to choose an efficient experimental design method [10].

Response surface method (RSM) is a combination of mathematical and statistical techniques. This method can be used to identify the influence and interaction of variables in the model, and reduce the complexity of the problem, and is often used to optimise parameters [11–13]. For example, Lorza et al. [14] obtained the best welding parameters for EN 235JR low carbon steel welded joints via RSM optimisation of speed, current and voltage. María et al. [15] optimised the galvanisation of steel screws by optimising the current density, temperature, deposition time and additive concentration. Tian et al. [16] used RSM on the heat treatment of wrought magnesium alloy and obtained a good strengthening effect.

Full factor design and Box–Behnken design are the two most commonly used RSM designs. However, full factor design requires a large amount of experimentation and is an expensive and time-consuming process. In contrast, Box–Behnken designs require fewer runs than a three-level factor design, so it is a more efficient way of designing experiments [17]. The Box–Behnken design method can analyse each level of testing for experimental factors. In a three-level factor system, when the factors are quantitative, the low, medium, and high levels are represented as -1, 0, and +1, respectively. This helps to fit a regression model that correlates response variables to factor levels [18]. For experimenters who are concerned with the curvature of the response function, a three-level factor design is certainly a possible choice. Therefore, in this paper, the Box–Behnken method is used to design the solid solution and ageing treatment for the Mg-13Gd-4Y-2Zn-0.5Zr alloy.

To promote the application of magnesium alloy in vibration and noise reduction engineering, this study makes a deep analysis on the damping performance of a novel advanced high-strength Mg-13Gd-4Y-2Zn-0.5Zr magnesium alloy by optimising the heat treatment process using Box–Behnken design method. The heat treatment parameters are solution temperature, solution time, ageing temperature and ageing time. The objective functions are the tensile strength and the mechanical damping coefficient, which is useful in engineering, rather than the damping capacity commonly used in theoretical research. The optimal heat treatment parameter combination is determined by the Box-Behnken design. The following heat treatment experiments based on the optimal parameters determined by the Box-Behnken design further verified that the best process is solution at 520 °C for 10 h followed by ageing at 239 °C for 22 h. The tensile strength reached 346.78 MPa and the damping coefficient reached 0.296. The microstructure, morphology and composition of the second phases after heat treatment were analysed by optical microstructure (OM), Scanning Electron Microscope (SEM), X-ray Diffraction (XRD) and Energy Dispersive Spectrometer (EDS). The volume fraction of the second phases was calculated by ImageJ software, and the blocking effect of second phases on dislocation movement was analysed to improve the vibration reduction performance of the material by controlling the microstructure during the heat treatment process.

2. Experimental

2.1. Damping Experiment

The chemical composition (wt %) of the investigated Mg-13Gd-4Y-2Zn-0.5Zr alloy is listed in Table 1. Rectangular specimens with dimensions of 65 mm × 6 mm × 2 mm were cut from the wrought Mg-13Gd-4Y-2Zn-0.5Zr shell.

The damping properties of the heat treated Mg-13Gd-4Y-2Zn-0.5Zr magnesium alloy were tested using a dynamic mechanical analyser (TA-DMA Q800, TA Instruments Inc, New Castle, DE, USA). Damping experiments used the double cantilever mode. The double cantilever fixture is shown in Figure 1 and the simplified model of double cantilever mode is shown in Figure 2. The test conditions were as follows: frequency of 1 Hz and strain amplitude of 8.8×10^{-5} to 2×10^{-2} at room temperature of 25 °C. The damping tests were carried out in triplicate for each sample. The resulting sinusoidal

force and deflection data were recorded and the damping capacities (Q^{-1}) can be evaluated by the loss tangent ($\tan\phi$), which is calculated using Equation (1).

$$Q^{-1} = \tan\phi = \frac{E'}{E''} \tag{1}$$

where E' is the loss modulus and E'' is the storage modulus.

For Equation (1), if $\tan\phi < 0.1$, the different expressions of damping property can be transformed into each other, as shown in Equation (2):

$$\tan\phi = Q^{-1} = \frac{\psi}{2\pi} \tag{2}$$

where ψ is the specific damping capacity (*SDC*).

In engineering, the damping coefficient, considering not only damping capacity but also the yield strength, can be calculated using ψ at 1/10 of the stress of the yield strength. In this paper, the mechanical damping performance is reported as the *SDC* of the material [19–21].

Table 1. Chemical composition (wt %) of Mg-13Gd-4Y-2Zn-0.5Zr alloy.

Mg	Gd	Y	Zn	Zr
Bal	13.77	4.64	2.39	0.29

2.2. Heat Treatment

For the solid solution treatment, temperatures of 420, 450, 480 and 510 °C and solid solution times of 4, 8, 12 and 16 h were selected for investigation. The cooling method is water cooling and the water temperature is about 70 °C.

For the ageing treatment, temperatures of 190, 210, 230 and 250 °C and ageing times of 12, 16, 20 and 24 h were chosen. Air cooling at room temperature was applied.

2.3. Microstructure Observation and Mechanical Properties Test

A Neophot2 optical microscope (OM, Zeiss, Oberkochen, Germany) and SU-5000 scanning electron microscope (SEM, Hitachi SU5000, Tokyo, Japan) were used to analyse the microstructure. The compositions of the phases and compounds in the alloy were analysed by energy dispersive spectroscopy (EDS, EDAX Inc, Mahwah, NJ, USA).

A DX-2700 X-ray diffraction (XRD, DX-2700, Dandong, China) analyzer was used to determine the phase of the sample. The parameters used were: scanning speed 5 °/min, scanning step 0.05°, scanning range 20–80°, acceleration voltage 40 KV, and filament current 30 mA.

An Instron 3382 static test machine (Instron Inc, Boston, MA, USA) was used for room temperature tensile testing.

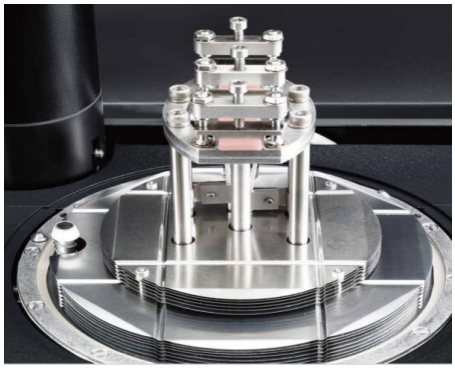

Figure 1. Double cantilever fixture.

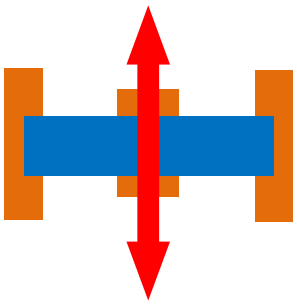

Figure 2. Simplified model of double cantilever mode.

3. Optimisation Analysis of Solid Solution Parameters

Figure 3 shows the damping–strain curves for the different solid solution treatments. It can be clearly seen that all the curves have been divided into two parts under different strains. Firstly, the value of Q^{-1} is low at low strain and there is a slight increment of Q^{-1} with increasing strain. This stage represents strain-independent damping (${Q_0}^{-1}$). Secondly, above the critical strain at about 0.001, the values of ${Q_H}^{-1}$ increase very quickly with increasing strain. On the basis of G-L damping theory, the action of dislocation segments bowing back and forth between weak pinning points generates the damping weakly dependent on strain amplitude. Once the strain amplitude exceeds the critical value, the dislocation breaks away from weak points and is finally pinned by point defects, and this process results in the formation of strain-dependent damping ${Q_H}^{-1}$[22].

As can be seen from the figure, when the solid solution temperature is 420 °C there is little change in the curves for all solid solution times. As the solid solution temperature increases, the damping performance of the alloy shows an increasing trend. With solid solution times of 8 h and 12 h, the resulting alloys have good damping performance. When the solution-ageing treatment was carried out at 510 °C for 12 h, the alloy achieved a higher damping performance value 0.0153.

Figure 4 shows the OM of the alloys, prepared at different solution temperatures with a solid solution time of 12 h. It can be seen that as the solution temperature increases, the grain size of the alloy grows significantly. The average grain size of the solution temperature 420, 450, 480 and 510 °C is 13.2, 23.6, 35.8 and 43.5 μm respectively. The grain boundary in the crystal is an effective obstacle to the dislocation motion. The grain size determines the total number of grain boundaries in the crystal, so the grain size has an effect on the dislocation motion. Sugimoto et al. [23] studied the effect of grain size on the damping properties of as-cast Mg-Ni alloys. It was found that as the grain size decreases and the number of grain boundaries increases, dislocation motion becomes difficult. Dislocations cannot be unpinned even under extreme stress, and the damping capacity is small.

It can also be seen from Figure 4 that there are still some second phases in solid solution Mg-13Gd-4Y-2Zn-0.5Zr alloy; this is mainly due to the high content of alloying elements. Figure 4a,b shows that with solution temperatures of 420 °C and 450 °C, there are some fine granular and lamellar phases inside the alloy, and the degree of solid solution is insufficient. Figure 4c,d shows that with solution temperatures of 480 °C and 510 °C, the amount of second phases in the alloy decreases, and the degree of solid solution is better. Zhen et al. [24] studied the influence of heat treatment on damping response of AZ91D magnesium alloy and concluded that the damping properties of AZ91D alloy under high strain conditions were improved after solution treatment. It is mainly because AZ91D alloy became a supersaturated solid solution as $Mg_{17}Al_{12}$ precipitation phases were decomposed during the solid solution treatment, and the number of strong pinning points for dislocation inside the grain is greatly reduced. Based on the data from Figures 3 and 4, a solid solution at 510 °C for 12 h is selected as the optimum solution parameter.

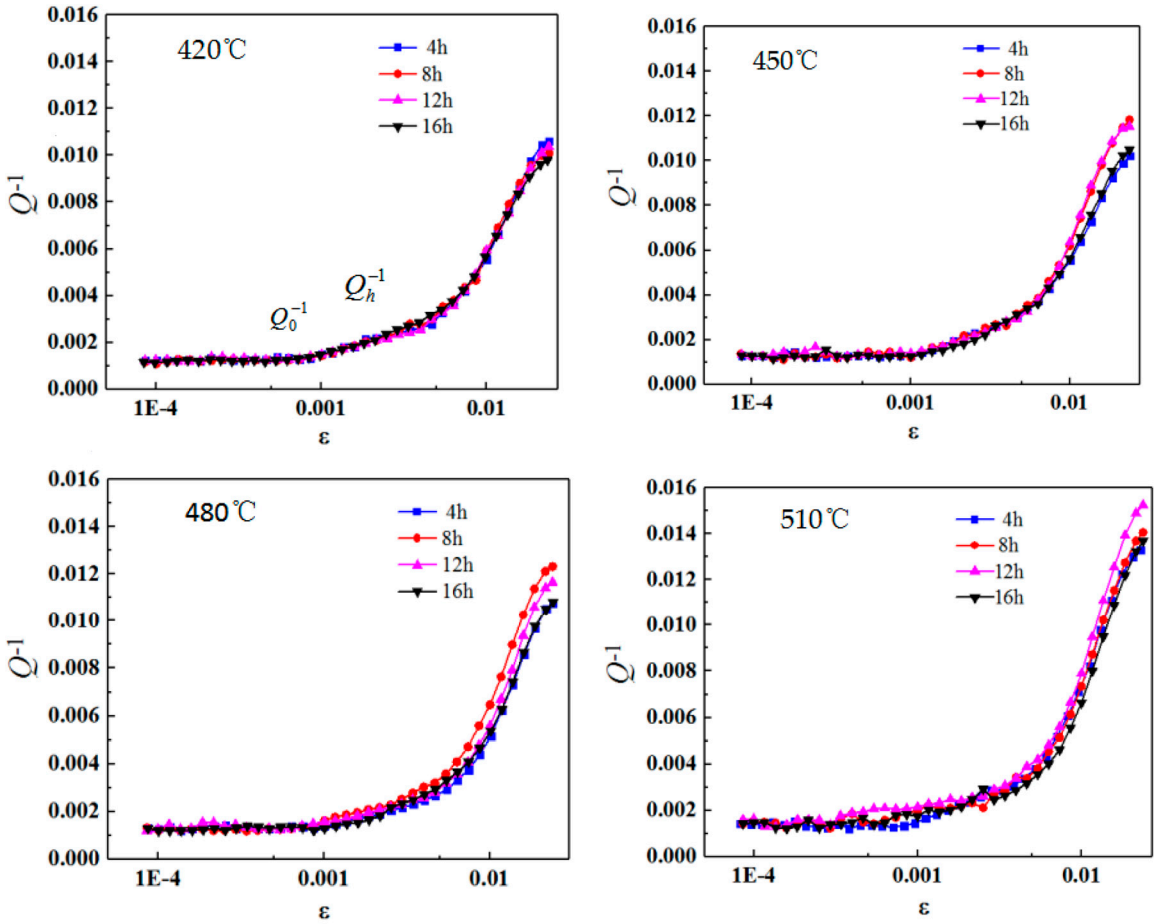

Figure 3. Damping–strain curves after different solid solution treatments.

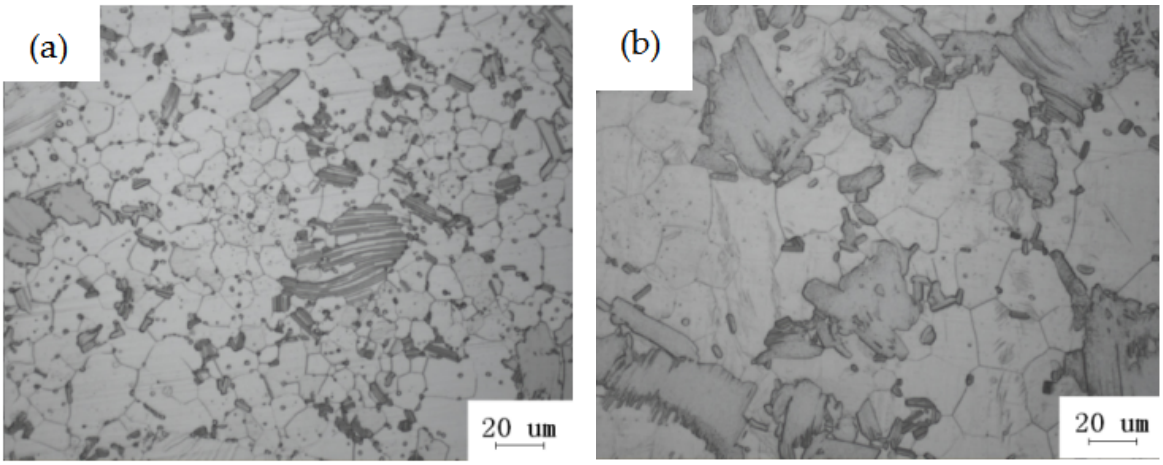

Figure 4. *Cont*.

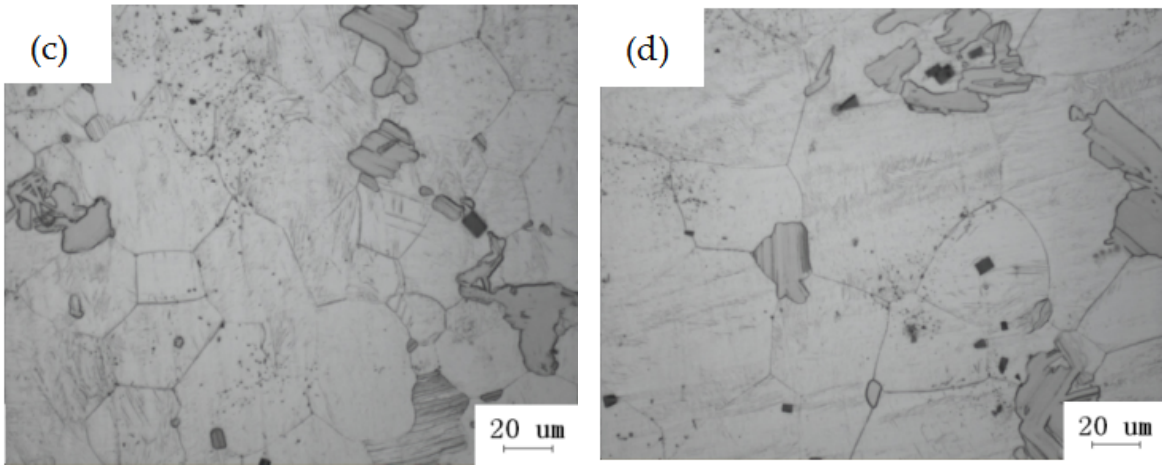

Figure 4. Optical microscopy (OM) images of the alloy after different solid solution treatments. (**a**) 420 °C × 12 h. (**b**) 450 °C × 12 h. (**c**) 480 °C × 12 h . (**d**) 510 °C × 12 h.

4. Optimisation Analysis of Ageing Parameters

Figure 5 shows the damping–strain curves for different ageing treatments. It can be seen that when the ageing temperature is 210 °C, the damping capacity of the alloy is lower than that of other ageing temperatures at different ageing times. When the ageing temperature is 190, 230, 250 °C, the damping performance of the alloy is higher when the ageing time is 20 h.

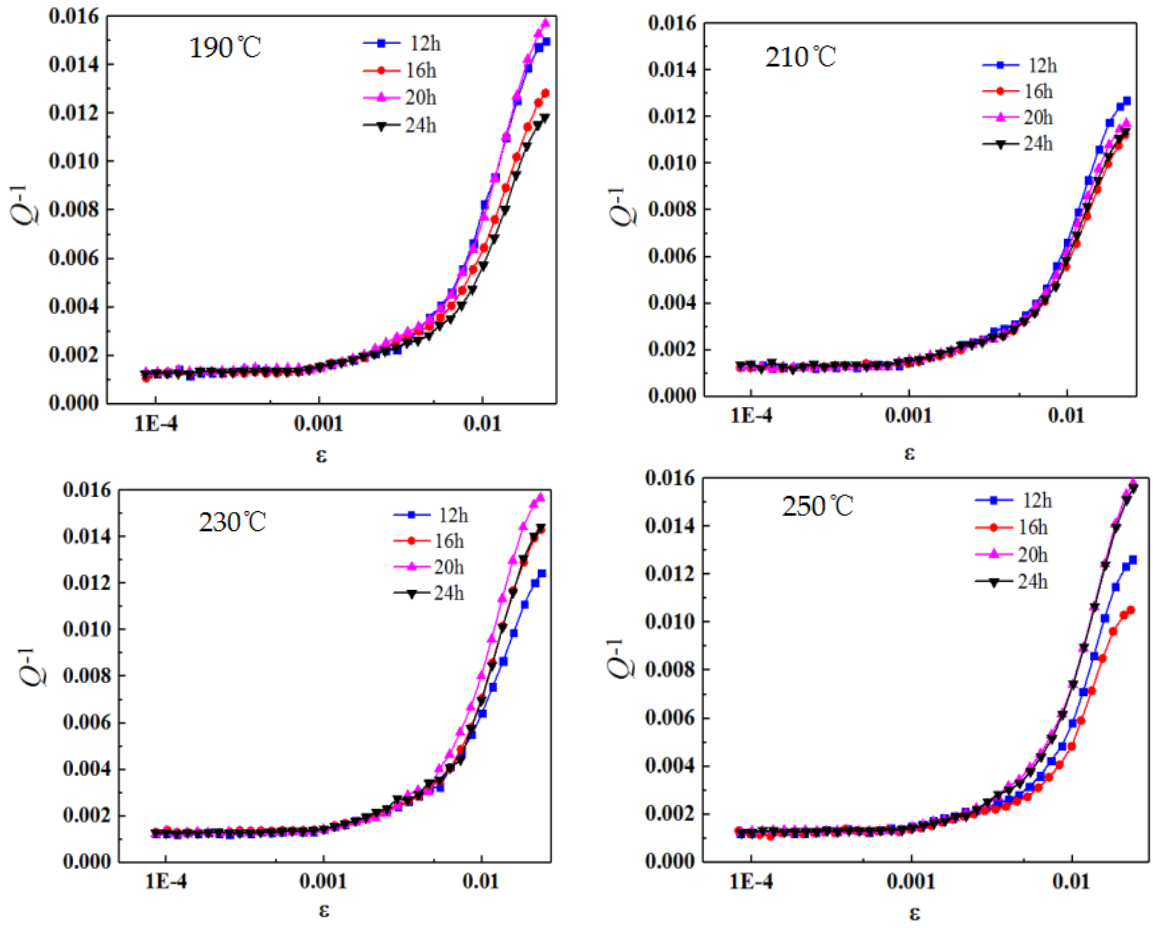

Figure 5. Damping–strain curves under different ageing treatments.

Figure 6 shows SEM images of the alloy at different ageing temperatures with an ageing time of 20 h. A large number of second phases with different shapes can be seen in Mg-13Gd-4Y-2Zn-0.5Zr alloys after the ageing treatment. It mainly includes granular phase, bulk LPSO (long period stacking ordered) phase, and some layer LPSO phase. The LPSO phase is an ordered structure in which the main components are RE and Zn atoms and they are placed periodically in the Mg basal planes [25–27]. As one important kind of Mg alloys, Mg-RE-Zn alloys (RE/Zn weight ratio >1, RE = Y, Gd, Tb, Dy, Ho, Er, Tm) have attracted great attention recently due to their enhanced properties by LPSO structure. Confirmed by researches, the LPSO phase could promote mechanical properties, corrosion resistance, damping capacity and other properties of Mg-alloys. Wang et al. [28] have ever investigated the mechanical properties and damping capacity of Mg-Zn-Zr alloys with varied second phases, including $MgZn_2$, $Mg_3Y_2Zn_3$,Mg_3YZn_6 and $Mg_{12}YZn$ (LPSO phase), and they found that LPSO phase could enhance mechanical properties and simultaneously optimise their damping capacities.

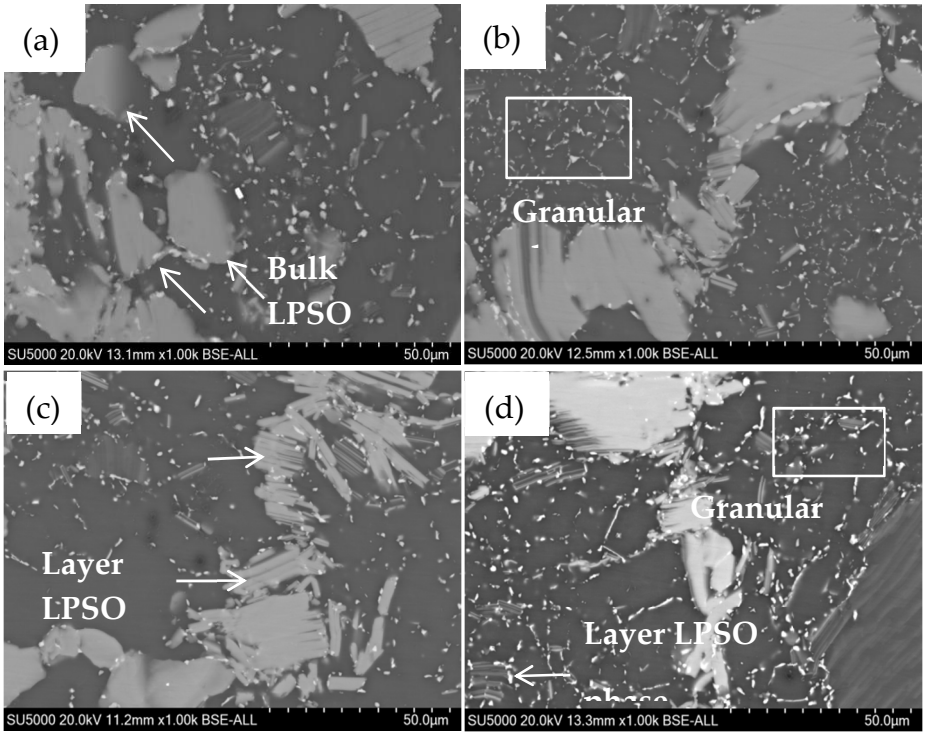

Figure 6. Scanning Electron Microscope (SEM) images of the alloy after different ageing treatments. (**a**) 190 °C × 20 h. (**b**) 210 °C × 20 h. (**c**) 230 °C × 20 h. (**d**) 250 °C × 20 h.

Figure 7 shows the XRD results for the alloy subjected to the 230 °C × 20 h ageing treatment. Clearly, the phase composition in the alloy after ageing treatment mainly includes three phases of α-Mg, $Mg_{12}YZn$ and Mg_5Gd. Figure 8 shows the EDS analysis of the alloy after different ageing treatments. Table 2 shows the results of the EDS analysis of the second phases in Figure 8. Take the sample of 190 °C × 20 h as an example, the cubic-shaped phase (Figure 8a, Spot ①) could be considered to be a RE-rich compound due to the EDS results. However, the RE-rich compound could not be analysed by XRD due to its low-volume fractions [29]. Two granular phases(Figure 8a, Spot ② and Spot ④) are considered to be the same phase due to their similar element content, and they may be Mg_5Gd [30]. But, the content of Mg is high due to the selected part of the matrix phase. The chemical composition of the block-shaped phase (Figure 8a, Spot ③) is Mg-3.62Gd-2.21Y-3.99Zn-0.26Zr (at. %), which indicates that the stoichiometry of this phase is near $Mg_{12}YZn$. Furthermore, the fine-lamellar phase (Spot ① in Figure 8b, Spot ③ in Figure 8c and Spot ③ in Figure 8d) emerged inside α-Mg grains, which should be an LPSO phase. So, these phases in Figure 8b (Spot ② and Spot ③) are Mg_5Gd, these phases in Figure 8c (Spot ① and Spot ②) are Mg_5Gd and $Mg_{12}YZn$, respectively, and these phases in Figure 8d

(Spot ① and Spot ②) Mg_5Gd and $Mg_{12}YZn$, respectively. According to the XRD and EDS results, the main component of the layer LPSO phase and the bulk LPSO phase is $Mg_{12}YZn$. The granular phase is mainly Mg_5Gd.

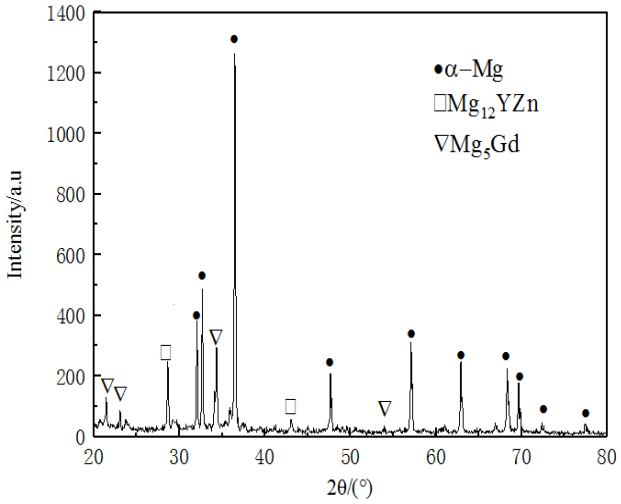

Figure 7. X-ray Diffraction (XRD) results for alloy subjected to 230 °C × 20 h ageing treatment.

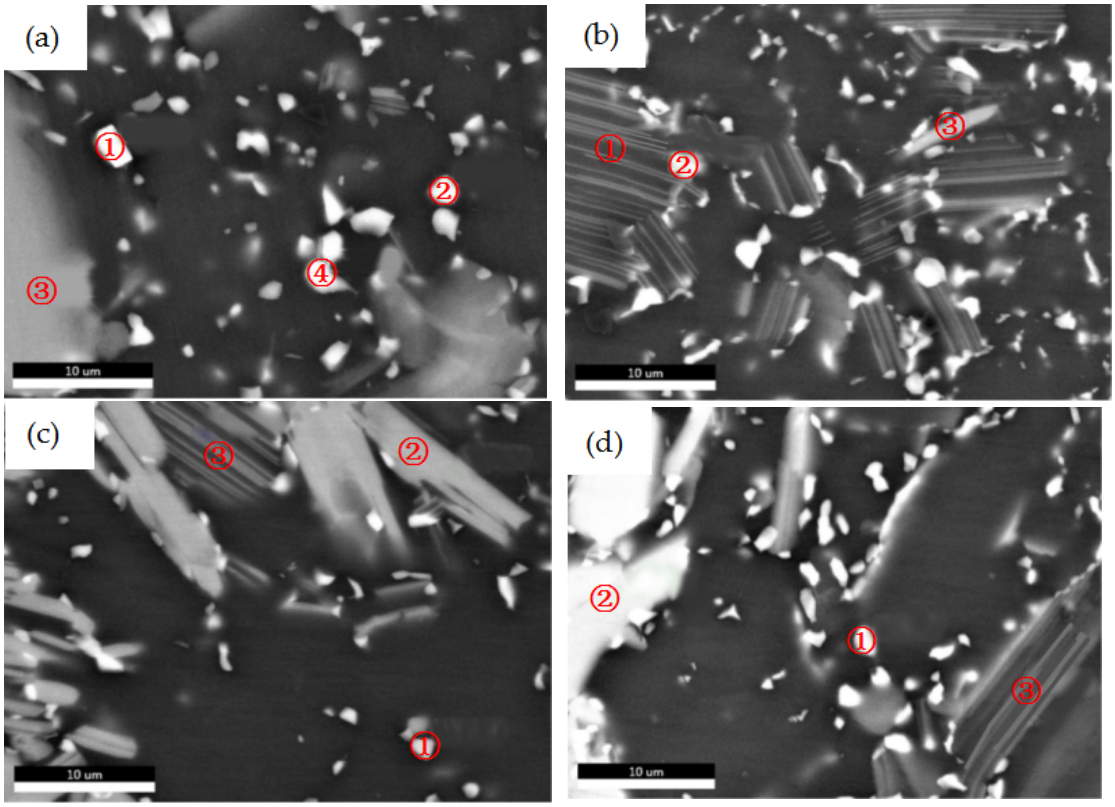

Figure 8. Energy Dispersive Spectroscopy (EDS) analysis selection map after different ageing treatments. (**a**) 190°C × 20 h. (**b**) 210°C × 20 h. (**c**) 230°C × 20 h. (**d**) 250°C × 20 h.

After the ageing treatment, there are a large number of second phases in Mg-13Gd-4Y-2Zn-0.5Zr alloys. Different shapes of phases have different obstructive effects on dislocation motion. In particular, the large-sized bulk phase will hinder the dislocation significantly. When the dislocation defect moves to the position of the bulk LPSO phase with a relatively large area, it will be "annihilated". Only when the dislocation defect moves to the position of granular phases in the vacant area other than the

massive bulk and layer phases, it will be pinned and unpinned under extreme stress. Therefore, the volume fraction of the second phases has an extreme effect on the damping capacity of ageing treated Mg-13Gd-4Y-2Zn-0.5Zr alloys. To further analyse the hindrance of the dislocation motion by second phases, statistical analysis was performed on the volume of the second phases shown in Figure 6 using ImageJ software. The software processing diagram is shown in Figure 9 and the statistical results are presented in Table 3.

Table 2. EDS results for the precipitated phases shown in Figure 8.

Sample	Detection Position	Element Content (at. %)					The Possible Phase
		Mg	Gd	Y	Zn	Zr	
190 °C × 20 h	Spot 1	56.01	20.70	21.02	0.65	1.63	RE-rich phase
	Spot 2	93.17	4.42	1.64	0.49	0.29	Mg_5Gd
	Spot 3	89.92	3.62	2.21	3.99	0.26	$Mg1_2YZn$
	Spot 4	91.80	5.40	1.85	0.66	0.29	Mg_5Gd
210 °C × 20 h	Spot 1	96.09	1.77	0.95	0.96	0.22	LPSO
	Spot 2	94.20	3.18	1.48	0.86	0.29	Mg_5Gd
	Spot 3	93.63	2.28	1.47	2.34	0.28	Mg_5Gd
230 °C × 20 h	Spot 1	94.25	3.54	1.42	0.52	0.28	Mg_5Gd
	Spot 2	90.65	3.23	1.90	3.94	0.28	$Mg_{12}YZn$
	Spot 3	93.70	2.49	1.30	2.23	0.27	LPSO
250 °C × 20 h	Spot 1	94.46	3.41	1.46	0.40	0.27	Mg5Gd
	Spot 2	88.76	3.84	2.46	4.64	0.30	$Mg_{12}YZn$
	Spot 3	96.89	1.63	0.76	0.51	0.21	LPSO

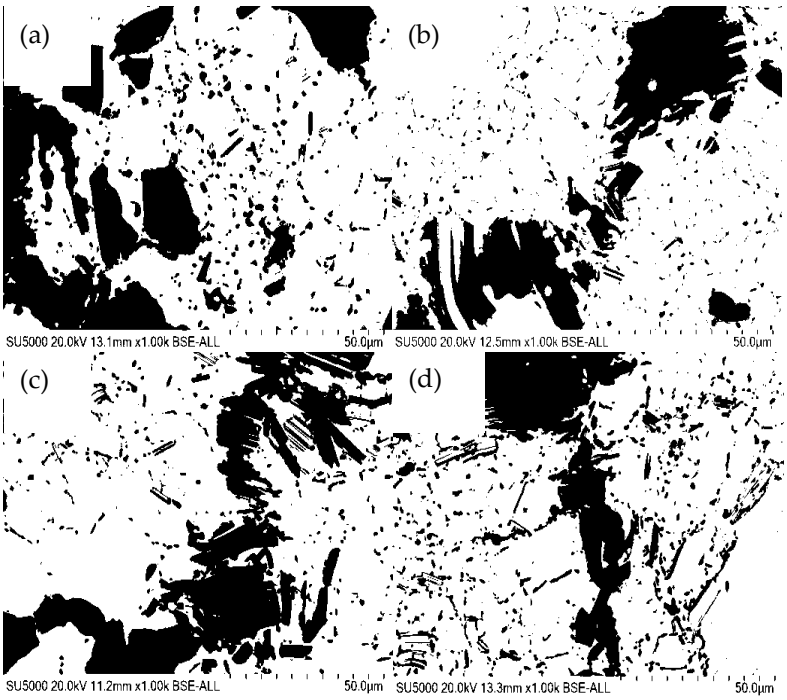

Figure 9. ImageJ software processing diagram for alloys subjected to different ageing treatments. (**a**) 190 °C × 20 h. (**b**) 210 °C × 20 h. (**c**) 230 °C × 20 h. (**d**) 250 °C × 20 h.

It can be seen from Table 3 that the 230 °C for 20 h ageing treatment results in the smallest volume fraction of the precipitated phases in the field of view. This indicates that the precipitated phases have the weakest hindrance to the movement of dislocation defects so that the alloy has the highest damping properties after the 230 °C for 20 h ageing treatment. From these results, and those shown in Figure 5, 230 °C for 20 h is chosen as the best ageing treatment.

Table 3. ImageJ software statistical results for alloy subjected to different ageing treatments as shown in Figure 9.

Ageing Treatment	190 °C × 20 h	210 °C × 20 h	230 °C × 20 h	250 °C × 20 h
Volume (Second phases)%	29.652	33.394	28.219	29.233

5. Mathematical Models

5.1. Design of Experiments

The solid solution temperature A, the solid solution time B, the ageing temperature C and the ageing time D are the design variables, while the tensile strength Y_1 and the mechanical damping coefficient Y_2 are the evaluation indexes. The solid solution condition of 510 °C for 12 h and the ageing condition of 230 °C for 20 h are selected as the value range for the design variables. The levels of the different variables in the experiment are shown in Table 4. The solid solution and ageing treatment experimental scheme and data calculation results are shown in Table 5.

Table 4. Levels of variables chosen for Box-Behnken Design.

Input	Notation	Level		
		−1	0	1
Solution temperature (°C)	A	495	510	525
Solution time (h)	B	10	12	14
Ageing temperature (°C)	C	215	230	245
Ageing time (h)	D	17	20	23

Table 5. Experimental scheme and data calculation results.

Experiment Number	Experimental Conditions				Yield Strength (MPa)	Calculated Parameters	
	Solution		Ageing				
	A (°C)	B (h)	C (°C)	D (h)		Y_1 (MPa)	Y_2
1	510	12	215	17	208.89	282.28	0.287
2	495	12	215	20	227.26	307.11	0.294
3	510	10	215	20	225.09	304.18	0.235
4	510	14	215	20	201.18	271.86	0.197
5	525	12	215	20	231.36	312.65	0.254
6	510	12	215	23	228.56	308.87	0.211
7	495	12	230	17	244.81	349.73	0.279
8	510	10	230	17	229.37	327.67	0.254
9	510	14	230	17	233.39	333.42	0.229
10	525	12	230	17	250.19	357.41	0.244
11	495	10	230	20	237.89	339.84	0.257
12	495	14	230	20	247.72	353.88	0.249
13	510	12	230	20	226.04	322.91	0.243
14	510	12	230	20	230.7	329.57	0.241
15	510	12	230	20	228.57	326.53	0.224
16	525	10	230	20	239.58	342.26	0.236
17	525	14	230	20	235	335.72	0.289
18	495	12	230	23	232.02	331.45	0.195
19	510	10	230	23	243.64	348.05	0.258
20	510	14	230	23	240.18	343.11	0.175
21	525	12	230	23	237.92	339.89	0.245
22	510	12	245	17	221.04	315.77	0.221
23	495	12	245	20	231.52	312.87	0.308
24	510	10	245	20	237.64	321.13	0.289
25	510	14	245	20	220.73	298.28	0.274
26	525	12	245	20	232.08	313.62	0.327
27	510	12	245	23	222.35	317.64	0.259

Taking samples 2 and 3 in Table 5 as an example, the damping coefficient is calculated as follows.

After the damping experiments, according to the data, the stress–strain fitting curves of samples 2 and 3 are shown in Figure 10. The damping–strain fitting curves of samples 2 and 3 are shown in Figure 11. The R values of the curves obtained in Figures 10 and 11 are both approximately 1, indicating that the fitting results are better.

The stress–strain fitting formulas are given as Equations (3) and (4).

$$y_1 = 343.44x_2 + 0.013 \tag{3}$$

$$y_2 = 358.14x_2 + 0.010 \tag{4}$$

Take 1/10 of the yield strength of the sample (22.73 MPa for sample 2 and 23.51 MPa for sample 3) and substitute Equations (3) and (4) to obtain the corresponding strain values and of 0.0661 and 0.0656, respectively [31].

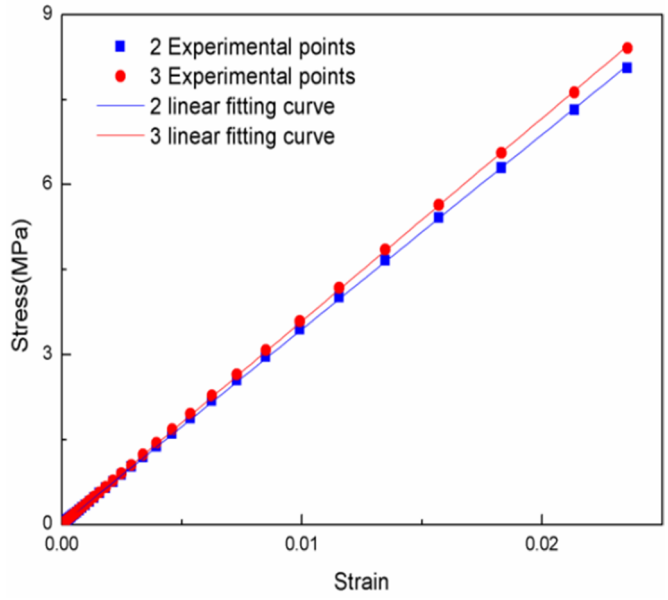

Figure 10. Stress–strain fitting curves for samples 2 and 3.

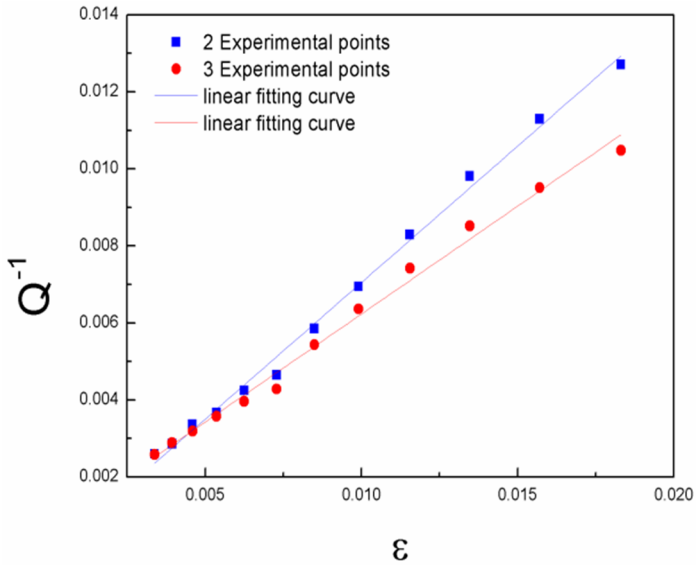

Figure 11. Damping–strain fitting curves for samples 2 and 3.

The damping–strain fitting formulas are given as Equations (5) and (6).

$$y_3 = 0.709x_3 - 3.94 \times 10^{-5} \quad (5)$$

$$y_4 = 0.560x_4 + 6.29 \times 10^{-4} \quad (6)$$

$$SDC = 2\pi Q^{-1} \quad (7)$$

Substituting the strain values into Equations (5) and (6), damping capacities of samples 2 and 3 are calculated as 0.0468 and 0.0374, respectively. Substituting into Equation (7), the damping coefficients of samples 2 and 3 are calculated to be 0.294 and 0.235, respectively.

5.2. Regression Analysis of Tensile Strength

The data in Table 5 were analysed using Design-Expert software (version8.05, Stat-Ease Inc, General Mills, Minneapolis, MN, USA) and the mathematical expression for the relationship between tensile strength and design variables is obtained as shown in Equation (8).

$$\begin{gathered} Y_1 = 8914.29685 - 60.68217A + 60.40250B + 56.03396C + 3.71713D - 0.17150AB + \\ 5.78889 \times 10^{-3}\mathrm{AC} + 4.22222 \times 10^{-3}AD + 0.078917BC - 0.44542BD - 0.13733CD + \\ 0.060104A^2 + 0.66115B^2 - 0.12332C^2 + 0.79231D^2 \end{gathered} \quad (8)$$

Variance analysis was performed on the above regression equation, and the results are shown in Table 6.

Table 6. Variance analysis results for the tensile strength equation.

Variables	Sum of Squares of Deviations	Degree of Freedom	Mean Square	*F*-Value	*p*-Value	Significant
Model	9167.77	14	654.84	4.18	0.0088	Extremely Significant
A	0.92	1	0.92	5.90×10^{-3}	0.9401	-
B	182.99	1	182.99	1.17	0.3011	-
C	565.26	1	565.26	3.61	0.0818	-
D	43.06	1	43.05	0.27	0.6097	-
AB	105.88	1	105.88	0.68	0.4271	-
dAC	6.79	1	6.79	0.043	0.8387	-
AD	0.14	1	0.14	9.21×10^{-4}	0.9763	-
BC	22.42	1	22.42	0.14	0.7119	-
BD	28.57	1	28.57	0.18	0.677	-
CD	152.77	1	152.77	0.97	0.343	-
A^2	975.36	1	975.36	6.22	0.0282	-
B^2	37.3	1	37.3	0.24	0.6344	-
C^2	4106.38	1	4106.38	26.2	0.0003	-
D^2	271.19	1	271.19	1.73	0.2129	-
Residuals	1880.66	12	156.72	-	-	-
Lack of fit	1858.43	10	185.84	16.72	0.0577	Not Significant
Pure Error	22.23	2	11.12	-	-	-
Total	11,048.43	26	-	-	-	-

Regression-Squared = 0.8298; Adjusted R-Squared = 0.6312; Adequate Precision = 6.771.

Statistically, the *p*-value is used to estimate the significance between response and design variables [32]. As can be seen from Table 6, the mathematical regression model has a *p*-value of 0.0088, which is less than 0.01. According to statistical regulation, the regression relationship between tensile strength and design variables is "extremely significant". Among the design variables, ageing temperature (*C*) has the lowest *p*-value of 0.0818, the correlation with tensile strength is the strongest, and *C* is the main effect item.

Lack of Fit is used to indicate how well the model used fits the experiment. As can be seen from Table 6, the *p*-value of Lack of Fit is 0.0577, which is greater than 0.05, the significance is "Not Significant", indicating that Equation (8) can be used to describe the relationship between tensile strength and design variables.

R-Squared represents the complex correlation coefficient of the regression equation and is used to evaluate the fitting effect of the mathematical model. The closer the Regression-value is to 1, the better the fitting effect. As can be seen from Table 6, the Regression-Squared is 0.8298, which indicates that the correlation between the fitted predicted value and the actual measured value is high, and the data of this fitting is relatively reliable.

Adequate Precision is used to measure the signal-to-noise ratio of the model, and its ideal value should be greater than 4. As can be seen from Table 6, the Adequate Precision is 6.771, which indicates that the model has sufficient resolution.

Based on the above analysis, the obtained regression Equation (8) can better describe the response of the objective function Y_1 with respect to the design variables A, B, C, and D, and the accuracy is better.

5.3. Regression Analysis of Damping Coefficient

The mathematical expression for the relationship between the damping coefficient and design variables is obtained as shown in Equation (9).

$$Y_2 = 53.93611 - 0.15012A - 0.24183B - 0.095844C - 0.30169D + 5.08333 \times 10^{-4}AB + 6.55556 \times 10^{-5}AC + 4.72222 \times 10^{-4}AD + 1.91667 \times 10^{-4}BC - 2.41667 \times 10^{-3}BD + 6.33333 \times 10^{-4}CD + 1.17222 \times 10^{-4}A^2 - 7.50000 \times 10^{-4}B^2 + 1.05556 \times 10^{-4}C^2 - 1.51389 \times 10^{-3}D^2 \quad (9)$$

The variance analysis was performed on the above regression equation, and the results are shown in Table 7.

Table 7. Variance analysis results for the damping coefficient equation.

Variables	Sum of Squares of Deviations	Degree of Freedom	Mean Square	*F*-Value	*p*-Value	Significant
Model	0.025	14	1.78×10^{-3}	2.69	0.0470	Significant
A	1.41×10^{-5}	1	1.41×10^{-5}	0.021	0.8864	-
B	1.12×10^{-3}	1	1.12×10^{-3}	1.69	0.2174	-
C	3.33×10^{-3}	1	3.33×10^{-3}	5.04	0.0444	-
D	2.44×10^{-3}	1	2.44×10^{-3}	3.68	0.0791	-
AB	9.30×10^{-4}	1	9.30×10^{-4}	1.41	0.2587	-
AC	8.70×10^{-4}	1	8.70×10^{-4}	1.32	0.2738	-
AD	1.81×10^{-3}	1	1.81×10^{-3}	2.73	0.1244	-
BC	1.32×10^{-4}	1	1.32×10^{-4}	0.2	0.6628	-
BD	8.41×10^{-4}	1	8.41×10^{-4}	1.27	0.2816	-
CD	3.25×10^{-3}	1	3.25×10^{-3}	4.91	0.0468	-
A^2	3.71×10^{-3}	1	3.71×10^{-3}	5.61	0.0355	-
B^2	4.80×10^{-5}	1	4.80×10^{-5}	0.073	0.7922	-
C^2	3.01×10^{-3}	1	3.01×10^{-3}	4.55	0.0543	-
D^2	9.90×10^{-4}	1	9.90×10^{-4}	1.5	0.2447	-
Residuals	7.94×10^{-3}	12	6.62×10^{-4}	-	-	-
Lack of fit	7.72×10^{-3}	10	7.72×10^{-4}	7.08	0.1299	Not Significant
Pure Error	2.18×10^{-4}	2	1.09×10^{-4}	-	-	-
Total	0.033	26	-	-	-	-

Regression-Squared = 0.7580; Adjusted R-Squared = 0.4757; Adequate Precision = 7.180.

As can be seen from Table 7, the mathematical regression model has a *p*-value of 0.0470, which is greater than 0.01 and less than 0.05. According to statistical regulation, the regression relationship between damping coefficient and design variables is "Significant". C is a significant item, the interactive item CD is a significant item, and C is the main effect item.

The *p*-value of Lack of Fit is 0.1299, which is greater than 0.05, the significance is "not significant", indicating that Equation (9) can be used to describe the relationship between damping coefficient and design variables.

The Regression-Squared is 0.7580, which indicates that the correlation between the fitted predicted value and the actual measured value is high, and the data of this fitting is relatively reliable.

The Adequate Precision is 7.180, which indicates that the model has sufficient resolution.

Based on the above analysis, the obtained regression Equation (9) can better describe the response of the objective function Y_2 with respect to the design variables A, B, C, and D, and the accuracy is better.

5.4. Parameter Optimisation

The mathematical regression model for the relationship between tensile strength and damping coefficient and design variables shows that the ageing temperature (C) is a significant term in the regression equation for the damping coefficient, and has the greatest influence on the tensile strength. Therefore, we will first determine the range of the ageing temperature, then discuss the influence of other factors on the objective function to analyse the interactions between experimental parameters.

Figures 12–14 are contour plots and response surface plots obtained after analysis of the tensile strength regression equation. The colour and shape of different areas in the contour map show the strength of the interaction. The darker the area, the more significant the effect of the interaction of the design variables on the response value [33,34]. Figure 12a shows that when the ageing temperature is in the range of 225–237 °C and the solid solution temperature is in the range of 495–500 °C or 520–525 °C, the interaction between the solid solution temperature and the ageing temperature is obvious, and a higher tensile strength of alloy is obtained. Correspondingly, in Figure 12b, when the interaction between the solution temperature and the ageing temperature is obvious, the slope of the curved surface becomes larger and the colour becomes darker.

In Figure 13a, the ageing temperature is between 227 and 237 °C and the solid solution time is between 10 and 11 h. The interaction is more obvious, and the tensile strength of the obtained alloy is larger. In Figure 14a, the ageing temperature is between 227 and 237 °C, and the ageing time is 17–18 h or 22–23 h, all of which result in an alloy with high tensile strength.

Figures 15–17 are contour plots and response surface plots obtained after analysis of the damping coefficient regression equation.

It can be seen from Figure 15a that the interaction is the most obvious when the solution temperature is 525 °C and the ageing temperature is 239–245 °C. The damping coefficient of the alloy reaches 0.32. Correspondingly, in Figure 15b, when the interaction between the solution temperature and the ageing temperature is obvious, the slope is steepest.

It can be seen from Figure 16a that the interaction between ageing temperature and solution time is not obvious during the solution-ageing heat treatment, and the solution time has little effect on the vibration-damping performance of the alloy. When the ageing temperature is 245 °C, the alloy has a large damping coefficient.

Figure 17a shows that with an ageing temperature of 239–245 °C and ageing time of 19–23 h, the best vibration damping performance is obtained.

In summary, through the analysis of the mathematical model established using Box–Behnken statistical method, the optimum heat treatment parameters are solid solution temperature 520 °C, solid solution time 10 h, ageing temperature 239 °C and ageing time 22 h. Under these heat treatment parameters, the tensile strength response is 328.21 MPa and the damping coefficient response is 0.287.

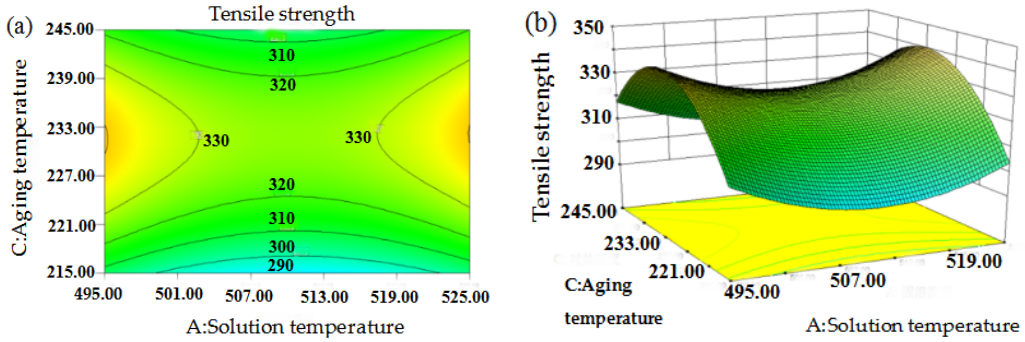

Figure 12. Interaction between ageing temperature and solution temperature versus the tensile strength. (**a**) contour map; (**b**) surface response map.

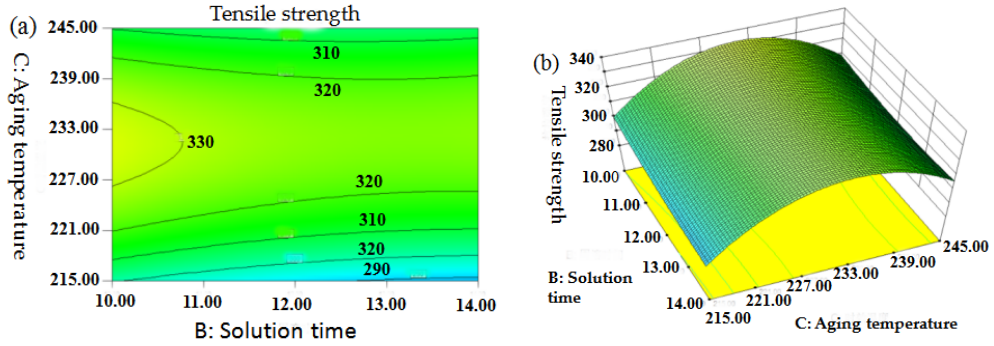

Figure 13. Interaction between ageing temperature and solution time versus the tensile strength. (**a**) contour map; (**b**) surface response map.

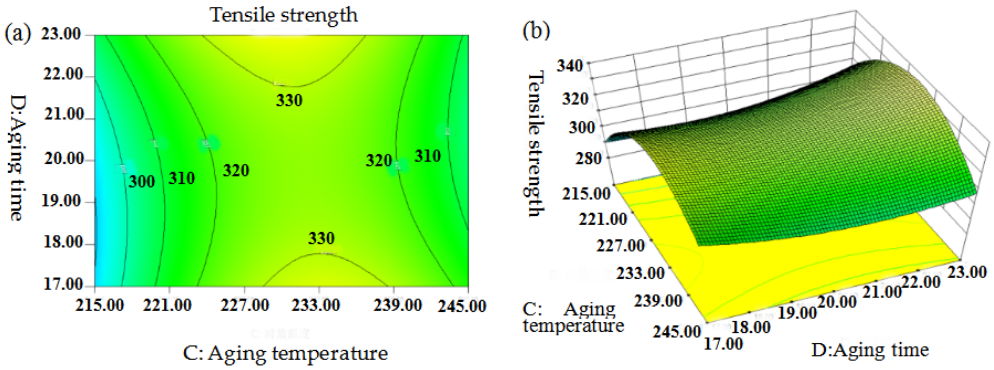

Figure 14. Interaction between ageing time and ageing temperature versus the tensile strength. (**a**) contour map; (**b**) surface response map.

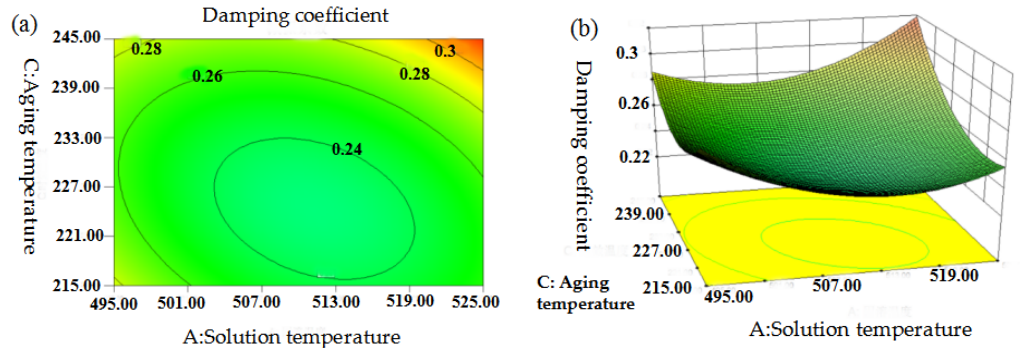

Figure 15. Interaction between ageing temperature and solution temperature versus the damping coefficient. (**a**) contour map; **(b)** surface response map.

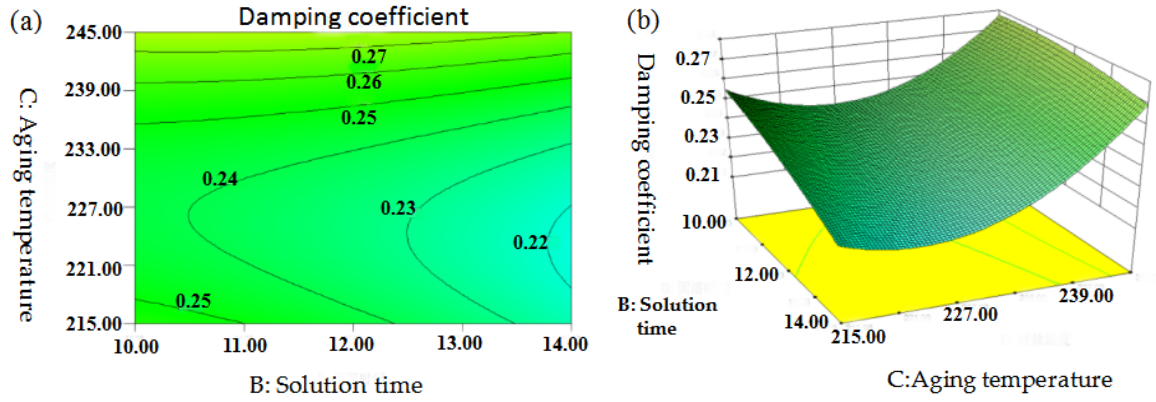

Figure 16. Interaction between ageing temperature and solution time versus the damping coefficient. (**a**) contour map; (**b**) surface response map.

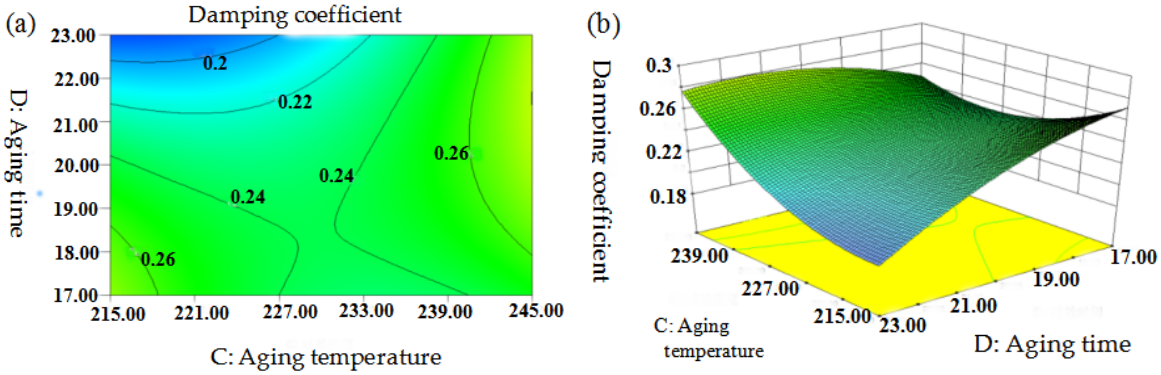

Figure 17. Interaction between ageing time and ageing temperature versus the damping coefficient. (**a**) contour map; (**b**) surface response map.

6. Verification Experiment

Using the optimal heat treatment parameters obtained using the Box–Behnken statistical method, five sets of solid solution and ageing heat treatment experiments were developed. Through DMA and mechanical properties tests, combined with microstructure analysis, the effects of the solid solution + ageing heat treatment processes on the vibration-damping performance of the alloy were analysed. The heat treatment process parameters, mechanical property test results and damping coefficient calculation results are reported in Table 8.

Table 8. Experimental parameters and results.

Sample	Heat Treatment	Tensile Strength (MPa)	Damping Coefficient
1	520 °C × 10 h + 239 °C × 22 h	346.78	0.296
2	520 °C × 10 h + 205 °C × 22 h	340.21	0.257
3	520 °C × 9 h + 230 °C × 20 h	298.53	0.247
4	520 °C × 11 h + 249 °C × 24 h	330.94	0.288
5	510 °C × 9 h + 230 °C × 20 h	317.33	0.252

The process parameters for sample 1 are the optimised parameters obtained from the Box–Behnken experimental method. From Table 8, sample 1 has the highest tensile strength and damping coefficient of 346.78 MPa and 0.296, respectively, which is slightly higher than those obtained by the Box–Behnken optimisation design. This shows the advancement and accuracy of the Box–Behnken optimisation design method. For sample 1, the mechanical damping coefficient is 0.296, which is 73.1% higher than the damping coefficient before heat treatment of 0.171. In addition, the highest damping capacity of sample 1, 2, 3, 4, 5 is 0.0152, 0.0136, 0.0132, 0.0162, 0.0131 respectively.

SEM microstructures of samples 1–5 are shown in Figure 18. It can be seen that the morphology of the second phases in the alloy differs depending on the heat treatment applied. There are mainly layer, short rod-shaped, bulk LPSO $Mg_{12}YZn$ and granular Mg_5Gd phases. As can be seen from Figure 18a,d, there are mainly layer, short rod-shaped LPSO $Mg_{12}YZn$ and granular Mg_5Gd phases, and Q^{-1} of the corresponding samples are higher. Moreover, as can be seen from Figure 18b,c,e, there are mainly bulk and little layer LPSO $Mg_{12}YZn$ and granular Mg_5Gd phases, and Q^{-1} of the corresponding samples are lower. It can be concluded that compared with the large bulk LPSO phase, the short rod-shaped LPSO phase effectively improves the damping performance of the alloy. It is mainly because the space between the short rod-like phases is larger, which is beneficial to the dislocation movement, while the space between the bulk phases is smaller, so the obstacle force to the dislocation motion is higher. Lu et al. [35] also found that the rod-like LPSO phase formed in Mg-Zn-Y alloy after heat treatment could improve the damping properties of the alloy. The rod-like LPSO phase balances the alloy's mechanical and damping properties.

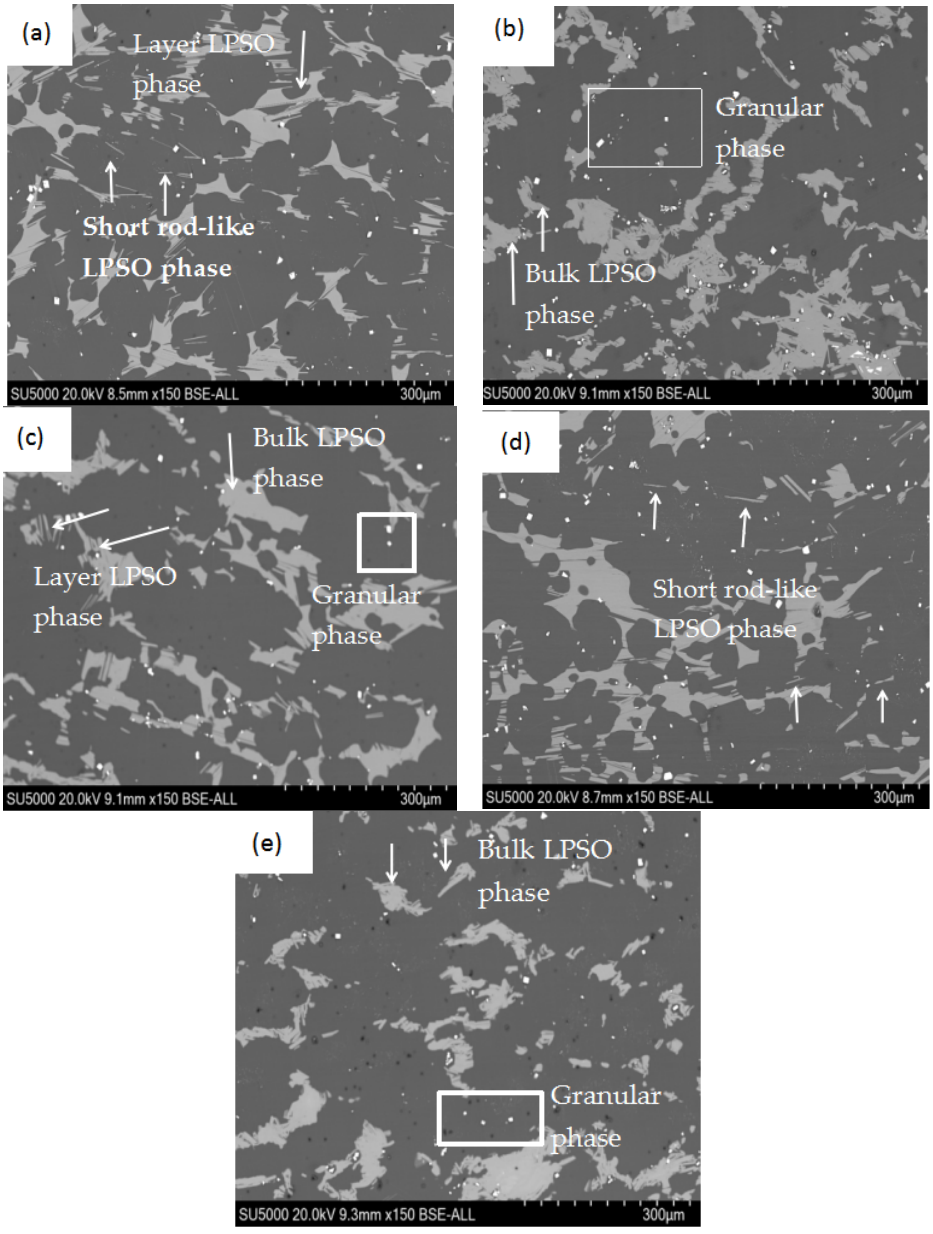

Figure 18. SEM microstructure of samples 1–5.(**a**) Sample 1; (**b**) Sample 2; (**c**) Sample 3; (**d**) Sample 4; (**e**) Sample 5.

As there are a lot of second phases in the alloy after heat treated, the volume of the second phases was also calculated by applying ImageJ software to process the SEM images shown in Figure 18. The statistical results are reported in Table 9.

It can be seen from Table 9 that the volume fraction of the second phases in the field of view is smaller in samples 1 and 4. The smaller the area occupied by the second phases, the larger the vacant area between the phases in the field of view, which indicates that the smaller the hindrance effect of the second phases as the pinning point on the motion of the dislocation defect, the better the mobility of the dislocation, and the better the damping capacity of the alloy. The statistical analysis results obtained using ImageJ software are consistent with the experimental results damping capacity.

Table 9. ImageJ software statistical results.

Sample	1	2	3	4	5
Volume (Second phases)%	17.104	20.973	22.31	16.322	17.463

7. Conclusions

The damping performance of a novel high-strength Mg-13Gd-4Y-2Zn-0.5Zr magnesium alloy was optimised using an efficient experimental design method, Box–Behnken method. The solid solution temperature A, the solid solution time B, the ageing temperature C and the ageing time D are the design variables, and the tensile strength Y_1 and the damping coefficient Y_2 (considering not only damping property but also the yield strength) are the evaluation indexes. First, the preliminary optimisation of the solid solution, ageing heat treatment parameters was carried out to determine the range of design variables respectively. Through analysis of the microstructure, second phases and damping curves, 510 °C × 12 h was selected as the optimum solid solution parameter, 210 °C × 20 h was chosen as the best ageing parameter. Then, through the analysis of the mathematical model established using the Box–Behnken statistical method, the optimum heat treatment parameters were found to be: solid solution temperature 520 °C, solid solution time 10 h, ageing temperature 239 °C and ageing time 22 h. Under these parameters, the tensile strength response was 328.21 MPa and the damping coefficient response was 0.287. According to the optimal heat treatment parameters obtained using the Box–Behnken method, five solid solution + ageing heat treatment experiments were developed. Among the obtained samples, sample 1 (520 °C × 10 h + 239 °C × 22 h) had the highest tensile strength of 346.78 MPa and damping coefficient 0.296, which is slightly higher than the tensile strength and damping coefficient obtained by the Box–Behnken optimization design. There was good agreement between the experimental and predicted results. There are a large number of second phases in Mg-13Gd-4Y-2Zn-0.5Zr alloys was found after heat treated, mainly due to the high content of alloying elements. They mainly include layer, short rod-shaped, bulk LPSO $Mg_{12}YZn$ and granular Mg_5Gd phases. It was found that the volume fraction of the second phases has an extreme effect on the damping capacity and short rod-shaped LPSO can effectively improve the damping capacity of heat-treated Mg-13Gd-4Y-2Zn-0.5Zr alloy. The volume fraction of the second phases was analysed by ImageJ software. It was concluded that the smaller the volume occupied by the second phases, the better the mobility of the dislocation, and the better the damping performance of the alloy. The statistical analysis results obtained using ImageJ software are consistent with the experimental results damping capacity.

Author Contributions: Conceptualization, J.Z., Z.K. and Y.Y.; Methodology, Y.Y. and B.L.; Software, X.L., Z.H. and M.Y.; Investigation, all authors; Writing—Original Draft Preparation, J.Z. and Y.Y.; Writing—Review and Editing, J.Z., Y.Y. and B.L.; Funding acquisition, Y.Y.

Funding: This work was sponsored by the National Natural Science Fund of China (Grant No.51775520), Shanxi Natural Science Fund (Grant No.201801D121110).

Acknowledgments: The Authors also thank the Magnesium-based deep processing technology in the engineering research of the Ministry of Education.

Conflicts of Interest: The authors declare no conflict of interest.

References

1. Wu, Y.W.; Wu, K.; Deng, K.K.; Nie, K.B.; Wang, X.J.; Zheng, M.Y.; Hu, X.S. Damping capacities and microstructures of magnesium matrix composities reinforced by graphite particles. *Mater. Des.* **2010**, *31*, 4862–4865. [CrossRef]
2. Granato, A.; Lücke, K. Theory of Mechanical Damping Due to Dislocations. *J. Appl. Phys.* **1956**, *27*, 583–593. [CrossRef]
3. Tang, Y.X.; Li, B.; Tang, H.X.; Xu, Y.C.; Gao, Y.P.; Huang, L.H.; Guan, J.Y. Effect of long period stacking ordered structure on mechanical and damping properties of as-cast Mg–Zn–Y–Zr alloy. *Mater. Sci. Eng. A* **2015**, *640*, 287–294. [CrossRef]
4. Lan, A.; Huo, L.F. Effect of substitution of minor Nd for Y on mechanical and damping properties of heat-treated Mg–Zn–Y–Zr alloy. *Mater. Sci. Eng. A* **2016**, *615*, 646–656. [CrossRef]
5. Yu, J.M.; Zhang, Z.M.; Zhang, X.; Ren, F.L.; Wu, Y.J. Study on microstructure evolution of deformed Mg-Gd-Y-Nd-Zr heat-resistant magnesium alloys after solid solution and ageing. *Sci. Sinter.* **2016**, *48*, 109–117. [CrossRef]
6. Yu, J.M.; Li, X.B.; Zhang, Z.M.; Wang, Q.; Wu, Y.J.; Wang, J. Mechanical behavior and microstructure evolution of Mg-Gd-Y-Zn-Zr alloy during multipass hot compression deformation. *Mater. Sci. Forum* **2016**, *849*, 186–195. [CrossRef]
7. Yu, J.M.; Zhang, Z.M.; Wang, Q.; Hao, H.Y.; Cui, J.Y.; Li, L.L. Rotary extrusion as a novel severe plastic deformation method for cylindrical tubes. *Mater. Lett.* **2018**, *215*, 195–199. [CrossRef]
8. Zhang, J.; Perez, R.J.; Lavemia, E.J. Effect of SiC and graphite particulates on the damping behavior of metal matrix composites. *Acta Metall. Mater.* **1994**, *42*, 395–409. [CrossRef]
9. Liu, X.L.; Chu, M.L.; Wen, Y.Z.; Hui, Z.L.; Su, M.Z. Effects of Homogenization Treatment on Microstructure and Properties of Mg-Zn-Nd-Cd-Zr Alloy. *Adv. Mater. Res.* **2011**, *11*, 76–79. [CrossRef]
10. Qin, X.P.; Wang, Y.L.; Lu, C.H.; Huang, S.; Zheng, H.; Shen, C.R. Structural acoustics analysis and optimization of an enclosed box-damped structure based on response surface methodology. *Mater. Des.* **2016**, *103*, 236–243. [CrossRef]
11. Abdulhadi, H.A.; Ahmad, S.N.A.S.; Ismail, L.; Ishak, M.; Mohammed, G.R. Experimental Investigation of Thermal Fatigue Die Casting Dies by Using Response Surface Modelling. *Metals* **2017**, *7*, 191. [CrossRef]
12. Sathish, T. BCCS Approach for the Parametric Optimization in Machining of Nimonic-263 alloy using RSM. *Mater. Today* **2018**, 14416–14422. [CrossRef]
13. Das, A.; Sarkar, S.; karanjai, M.; Sutradhar, G. RSM Based Study on the Influence of Sintering Temperature on MRR for Titanium Powder Metallurgy Products using Box-Behnken Design. *Mater. Today* **2018**, *5*, 6509–6517. [CrossRef]
14. Lorza, R.L.; García, R.E.; Calvo, M.A.M.; Vidal, R.M. Improvement in the Design of Welded Joints of EN 235JR Low Carbon Steel by Multiple Response Surface Methodology. *Metals* **2016**, *6*, 205. [CrossRef]
15. Lorza, R.L.; Calvo, M.A.M.; Labari, C.B.; Fuente, P.R. Using the Multi-Response Method with Desirability Functions to Optimize the Zinc Electroplating of Steel Screws. *Metals* **2018**, *8*, 71. [CrossRef]
16. Tian, Z.K.; Zhang, Z.M.; Yu, J.M.; Yu, H.T.; Yang, Y.Q. Influence of Heat Treatment on Microstructure and Mechanical Properties of Large Deforming and Heat-resisting Magnesium Alloys. *New Technol. New Process* **2016**, *4*, 76–78. [CrossRef]
17. Sahu, U.K.; Mahapatra, S.S.; Patel, R.K. Application of Box-Behnken Design in response surface methodology for adsorptive removal of arsenic from aqueous solution using CeO2/Fe2O3/graphene nanocomposite. *Mater. Chem. Phys.* **2018**, *207*, 233–242. [CrossRef]
18. Sadoun, O.; Rezgui, F.; G'Sell, C. Optimization of valsartan encapsulation in biodegradables polyesters using Box-Behnken design. *Mater. Sci. Eng. C* **2018**, *90*, 189–197. [CrossRef] [PubMed]
19. Niua, R.L.; Yana, F.J.; Wang, Y.S.; Duana, D.P.; Yang, X.M. Effect of Zr content on damping property of Mg–Zr binary alloys. *Mater Sci. Eng. A* **2018**, *718*, 418–426. [CrossRef]
20. Jun, J.H. Damping behavior of Mg–Zn–Al casting alloys. *Mater Sci. Eng. A.* **2016**, *665*, 86–89. [CrossRef]
21. Wan, D.Q.; Wang, J.C. Internal Friction Peaks in Mg-0.6% Zr and Mg-Ni High Damping Magnesium Alloys. *Rare Met. Mater. Eng.* **2017**, *46*, 2790–2793. [CrossRef]

22. Wang, J.F.; Lu, R.P.; Wei, W.W.; Huang, X.F.; Pan, F.S. Effect of long period stacking ordered(LPSO) structure on the damping capacities of Mg-Cu-Mn-Zn-Y alloys. *J. Alloys Compd.* **2012**, *527*, 1–5. [CrossRef]
23. Sugimoto, K.; Niiya, K.; Okamoto, T.; Kishitake, K. Study of damping capacity in Magnesium alloys. *Trans. Jpn. Inst. Met.* **1977**, *18*, 277–288. [CrossRef]
24. Zhen, Y.Z.; Xiao, Q.Z.; Wen, J.J. The influence of heat treatment on damping response of AZ91D magnesium alloy. *Mater. Sci. Eng. A* **2005**, *392*, 150–155. [CrossRef]
25. Lv, B.J.; Peng, J.; Zhu, L.L.; Wang, Y.J.; Tang, A.T. The effect of 14H LPSO phase on dynamic recrystallization behavior and hot workability of Mg–2.0Zn–0.3Zr–5.8Y alloy. *Mater. Sci. Eng. A* **2014**, *599*, 150–159. [CrossRef]
26. Tahreen, N.; Zhang, D.F.; Pan, F.S.; Jiang, X.Q.; Li, C.; Li, D.Y.; Chen, D.L. Characterization of hot deformation behavior of an extruded Mg–Zn–Mn–Y alloy containing LPSO phase. *J. Alloys Compd.* **2015**, *644*, 814–823. [CrossRef]
27. Yu, J.M.; Zhang, Z.M.; Wang, Q.; Yin, X.Y.; Cui, J.Y. Dynamic recrystallization behavior of magnesium alloys with LPSO during hot deformation. *J. Alloys Compd.* **2017**, *704*, 382–389. [CrossRef]
28. Wang, J.F.; Gao, S.; Song, P.F.; Huang, X.F.; Pan, F.S. Effects of phase composition on the mechanical properties and damping capacities of as-extruded Mg-Zn-Y-Zr alloys. *J. Alloys Compd.* **2001**, *509*, 8567–8572. [CrossRef]
29. Zhang, G.S.; Zhang, Z.M.; Du, Y.; Yan, Z.M.; Che, X. Effect of Isothermal Repetitive Upsetting Extrusion on the Microstructure of Mg-12.0Gd-4.5Y-2.0Zn-0.4Zr Alloy. *Materials* **2018**, *11*, 2092. [CrossRef]
30. Zhang, Z.M.; Yan, Z.M.; Du, Y.; Zhang, G.; Zhu, J.; Ren, L.; Wang, Y. Hot Deformation Behavior of Homogenized Mg-13.5Gd-3.2Y-2.3Zn-0.5Zr Alloy via Hot Compression Tests. *Materials* **2018**, *11*, 2282. [CrossRef]
31. Shanavas, S.; Dhas, J.E. Parametric optimization of friction stir welding parameters of marine grade aluminium alloy using response surface methodology. *Trans. Nonferrous Met. Soc.* **2017**, *27*, 2334–2344. [CrossRef]
32. Bhuyan, R.K.; Mohanty, S.; Routara, B.C. RSM and Fuzzy logic approaches for predicting the surface roughness during EDM of Al-SiCp MMC. *Mater. Today* **2017**, *4*, 1947–1956. [CrossRef]
33. Afshar, S.; Banisadi, H. Investigation the effect of graphene oxide and gelatin/starch weight ratio on the properties of starch/gelatin/GO nanocomposite films: The RSM study. *Int. J. Biol. Macromol.* **2018**, *109*, 1019–1028. [CrossRef] [PubMed]
34. Solmaz, S.; Raei, E.; Talebbeydokhti, N. Enhanced removal of phosphate from aqueous solutions using a modified sludge derived biochar: Comparative study of various modifying cations and RSM based optimization of pyrolysis parameters. *J. Environ. Manag.* **2018**, *225*, 75–83. [CrossRef]
35. Lu, R.P.; Song, P.F.; Huang, S.; Pan, F.S. Effects of heat treatment on the morphology of long-period stacking ordered phase and the corresponding mechanical properties of Mg–9Gd–xEr–1.6Zn–0.6Zr magnesium alloys. *Mater. Sci. Eng. A* **2013**, *2*, 36–45. [CrossRef]